Title: Somatosensory cortex microstimulation modulates primary motor and premotor cortex neurons with extensive spatial convergence and divergence

Abbreviated Title: S1-ICMS effects in M1 and PM

Authors: Brandon Ruszala[1], Kevin A. Mazurek[2,3,4], and Marc H. Schieber[1,2,3*]

Affiliations:
[1]Department of Biomedical Engineering, University of Rochester, Rochester, NY, 14627
[2]Department of Neurology, University of Rochester, Rochester, NY, 14642
[3]Department of Neuroscience, University of Rochester, Rochester, NY 14642
[4]Department of Neurology, Mayo Clinic, Rochester, MN, 55905

***Corresponding Author:** Please address correspondence to:
Marc H. Schieber
Department of Neurology
University of Rochester Medical Center
601 Elmwood Avenue, Box 673
Rochester, NY 14642
E-mail: mschiebe@ur.rochester.edu

Highlights

- Somatosensory cortex microstimulation modulated motor and premotor cortex neurons.
- Inhibitory effects were more common than excitatory effects.
- Effects from stimulation on each ~2x2 mm multielectrode array diverged widely.
- Effects in individual neurons converged from multiple somatosensory arrays.

eTOC blurb

Ruszala and colleagues show that multi-channel intracortical microstimulation in a small patch of somatosensory cortex modulates neurons distributed widely in both the primary motor and premotor cortex, with more effects being inhibitory than excitatory. Such modulation may complicate decoding motor intent when artificial sensation is delivered in bidirectional brain-computer interfaces.

Graphical Abstract

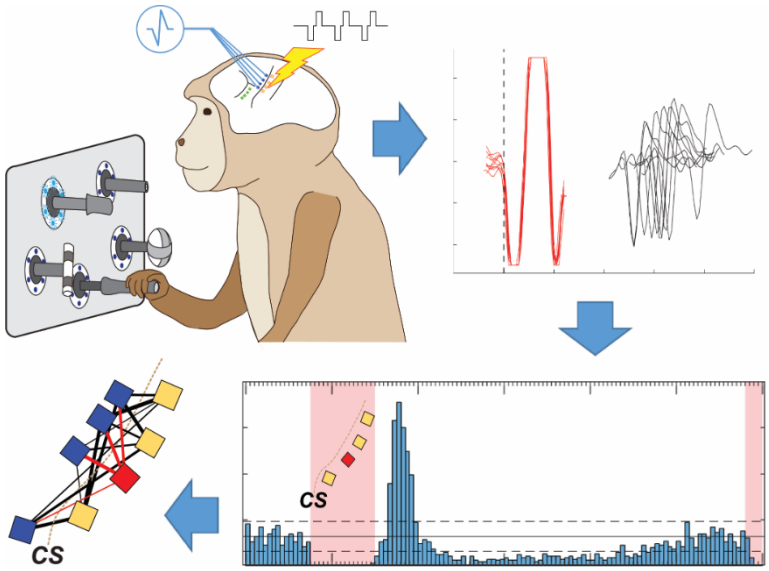

Summary

Although intracortical microstimulation (ICMS) can affect distant neurons transynaptically, the extent to which ICMS pulses delivered in one cortical area actually modulate neurons in other cortical areas during voluntary behavior remains largely unknown. Here, we assessed how the individual pulses of multi-channel ICMS trains delivered in the primary somatosensory cortex (S1) modulate neuron firing in the primary motor (M1) and premotor (PM) cortex. S1-ICMS pulses modulated the majority of units recorded in both M1 and PM, producing more inhibition than excitation. Effects converged on individual neurons in both M1 and PM from extensive S1 territories. Conversely, effects of ICMS in a small region of S1 diverged to wide territories in both M1 and PM. Our findings may have ramifications for development of bidirectional brain-computer interfaces, where ICMS used to deliver artificial feedback in S1 could modulate the activity of neurons in M1 and PM, thereby hindering decoding of motor intent.

Keywords

Brain-computer interface, Brain stimulation, Instruction, Intracortical microstimulation, Excitation, Inhibition, Reach, Grasp, Manipulate

Introduction

Intracortical microstimulation (ICMS) injects microampere current pulses into cortical gray matter, exciting neural elements in the vicinity of the electrode tip. Early work examining the radius of activation estimated that a single 40 µA pulse directly excited neuron somata up to 400 µm away (Stoney et al., 1968). Transsynaptic activation of more distant cortical neurons initially was thought to be rare, leading to the common assumption that ICMS excites only neurons within a few hundred micrometers of the stimulating electrode. However, subsequent studies have demonstrated that ICMS pulses also excite local axons, activating cortical neurons at extended distances both antidromically and orthodromically (Histed et al., 2009). Moreover, orthodromic action potentials, evoked in both somata and axons, can produce transsynaptic excitation of additional neurons that becomes particularly prominent when ICMS pulses are delivered in high-frequency trains, enabling temporal summation of successive excitatory postsynaptic potentials (Hussin et al., 2015; Jankowska et al., 1975).

Such transsynaptic activation can occur well beyond the cortical locale of the electrode. Single pulses delivered in the ventral premotor cortex (PMv), for example, excite corticospinal neurons in the primary motor cortex (M1) (Maier et al., 2013), and trains of ICMS delivered in M1 excite spinal motoneurons (Andersen et al., 1975; Asanuma and Ward, 1971). Although the effects of ICMS can extend well beyond the stimulated cortical region, few studies have examined how ICMS delivered in one cortical region modulates neural activity in other cortical regions. Understanding the cortico-cortical effects of ICMS, in addition to advancing our knowledge of how ICMS influences brain activity (Mazurek and Schieber, 2019; Mazurek and Schieber, 2021), may have practical applications. In bidirectional brain-computer interfaces (Flesher et al., 2021; O'Doherty et al., 2011; Pandarinath and Bensmaia, 2022), for example, ICMS delivered in the primary somatosensory cortex (S1) to provide tactile feedback might directly modulate the discharge of M1 neurons being used to decode movement intent. Such artificially induced modulation could reduce the performance of a decoding algorithm that uses the activity of those M1 neurons as inputs (Shelchkova et al., 2022). Here, we tested the hypothesis that ICMS pulses delivered in primary somatosensory cortex (S1-ICMS) directly modulate the firing of neurons in two cortical motor areas known to receive somatosensory input—M1 (Fetz et al., 1980; Lemon and Porter, 1976; Rosen and Asanuma, 1972; Wong et al., 1978), and PM (Gentilucci et al., 1988; Rizzolatti et al., 1988). We then examined the spatial distribution of the modulation that S1-ICMS produced in each of these cortical motor areas.

Results

We analyzed data recorded during a previously reported study in which two male rhesus macaque monkeys (L and X) initially were trained to perform four reach-grasp-manipulation (RGM) movements instructed with visual (LED) cues, and subsequently were trained to perform the same RGM task instructed instead with trains of ICMS pulses (Mazurek and Schieber, 2017). Each of the four different RGM movements was instructed by ICMS delivered simultaneously through multiple electrodes on a single ~2x2 mm microelectrode array implanted in S1, with different movements instructed by stimulation through different arrays. The present results are based on recordings made after each monkey was well-trained to use such ICMS instructions delivered in S1. Ultimately, trials with only visual instructions or only ICMS instructions could be interleaved randomly and the monkeys each continued to perform well, successfully completing >86% of the visually-instructed trials and >73% of the ICMS-instructed trials. All data used in the present analyses were recorded in sessions consisting entirely of such

randomly interleaved visually- versus ICMS-instructed trials. Four such recording sessions were analyzed from monkey L and three sessions from monkey X.

During each session, neuron spiking data were collected from other 16-channel microelectrode arrays implanted in M1 and PM of each monkey. After off-line sorting, each sorted waveform was classified as a definite single unit (DSU), probable single unit (PSU), or multi-unit (MU) according to criteria described in the Methods. Units were tracked across consecutive days based on their mean waveforms, mean firing rates, autocorrelograms, and cross-correlograms with other units (Fraser and Schwartz, 2012). Units found to be present in multiple sessions were analyzed only once, from the first session in which they appeared. In Monkey L, 81 units were analyzed – 38 from M1 and 42 from PM. The 38 M1 units were comprised of 9 DSUs, 8 PSUs, and 21 MUs. The 42 PM units were comprised of 5 DSUs, 12 PSUs, and 25 MUs. In Monkey X, 69 units were analyzed – 36 from M1 and 33 from PM. The 36 M1 units were comprised of 6 DSUs, 14 PSUs, and 16 MUs. The 33 PM units were comprised of 2 DSUs, 6 PSUs, and 25 MUs. Units of all three types were included in the following analyses unless stated otherwise.

Direct modulation of neurons in M1 and PM produced by S1-ICMS

Figure 1 displays four PSTHs constructed with spikes from the same definite single unit recorded in M1. Each PSTH was triggered on the artifacts of ICMS pulses from one of the four ICMS instructions, each delivered via electrodes on a different S1 array. Whereas the ICMS pulses of instructions 1 and 4 did not modulate this neuron's discharge (Fig. 1A, 1D), the ICMS pulses of instructions 2 and 3 did, producing different patterns of peaks and/or troughs in their respective PSTHs (Fig. 1B, 1C). We refer to such evidence of increased and/or decreased spike probability as "direct modulation."

ICMS instructions delivered through electrodes on the four different S1 arrays in each monkey provided 152 M1 neuron-array pairs and 168 PM pairs in monkey L; 144 M1 pairs and 132 PM pairs in monkey X. The pairs involving one S1

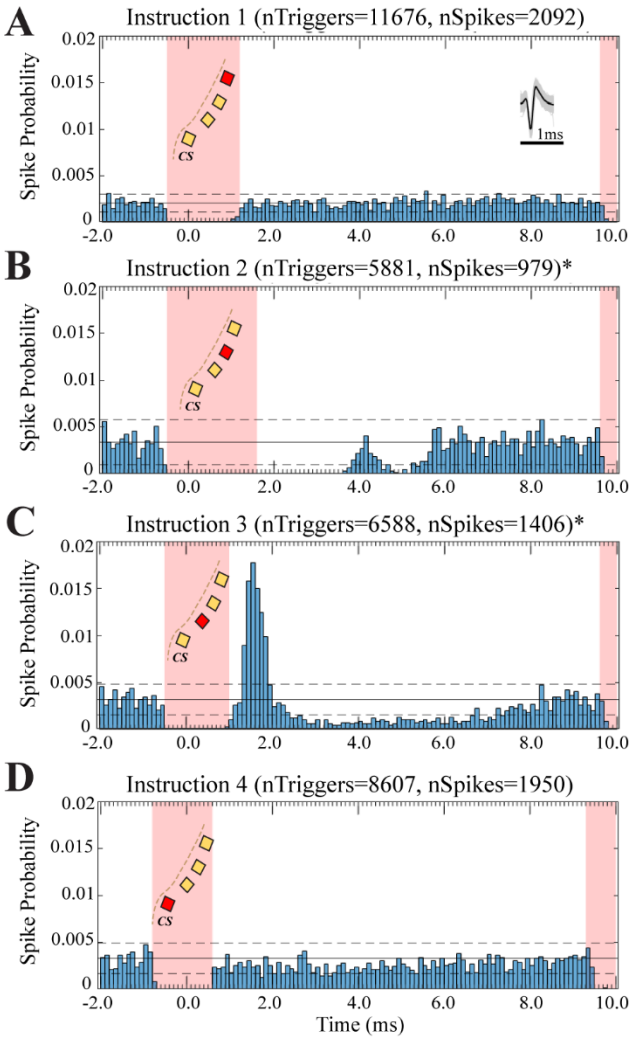

Figure 1. Peristimulus time histograms triggered on ICMS pulse artifacts from the instruction for each target object. *All four PSTHs show spikes from the same definite single unit in M1, triggered on ICMS pulse artifacts from the* ***A)*** *button,* ***B)*** *sphere,* ***C)*** *perpendicular cylinder, or* ***D)*** *coaxial cylinder instruction. Spike counts in each 0.1 ms bin were converted to probabilities by dividing the count in each bin by the number of ICMS pulse artifacts used as triggers to form the PSTH (nTriggers). Pink rectangles show the artifact window during which spikes could not be reliably discriminated. Horizontal black lines represent the mean (solid line) ± 2 standard deviations (dashed lines) of the baseline bins preceding the first artifact window. The average waveform of the unit is shown in the upper right corner of the PSTH, with overlapped individual spikes in gray and a 1 ms timescale bar below in black. Note that the baseline firing probability varied among the four PSTHs because the neuron fired differently during trials involving the four different objects. Ch109U1, L, 20150729*

array in monkey X were excluded from analysis, however, because the high stimulation frequency used for that array (225 Hz) resulted in inter-pulse intervals (4.4 ms) too short for reliable assessment of modulation. The remaining 108 M1 and 99 PM neuron-array pairs from monkey X were included in the subsequent analyses.

For M1 neurons, we identified at least one peak or trough that exceeded ± 2 standard deviations of the pre-stimulus baseline (see Methods) in the PSTHs of 85/152 (55.9%) neuron-array pairs from monkey L and 44/108 (40.7%) pairs from monkey X; for PM neurons, 45/168 (26.8%) pairs from monkey L and 35/99 (35.4%) pairs from monkey X. We also assessed the percentage of neurons that were directly modulated by ICMS delivered through electrodes on at least one S1 array. For M1 neurons, 33/38 (87%) in monkey L and 28/36 (78%) in monkey X were directly modulated by ICMS delivered on at least one S1 array; for PM neurons, 26/42 (62%) in monkey L and 29/33 (88%) in monkey X. The majority of neurons recorded in both M1 and PM were directly modulated by ICMS delivered on at least one S1 array.

Combining the data from the two monkeys, we identified 46 peaks in M1 and 44 in PM; 162 troughs in M1 and 77 in PM. The frequencies of peaks vs. troughs differed in M1 vs PM (X^2-test, p = 0.0052). Overall, inhibition was more common than excitation, more so in M1 than in PM.

Although single peaks or troughs were most frequent, many PSTHs showed multiple effects, as exemplified by the two troughs in Fig. 1B or the peak and trough in Fig. 1C. Table 1 gives the numbers of PSTHs with single peaks, single troughs, or multiple effects in M1, in PM, and in the two areas combined, each broken down by whether the neuron was a DSU, PSU, or MU. We considered the possibility that MUs might be more likely to show multiple effects, but pooling the effects from M1 and PM showed no dependence between unit quality and single peak vs. single trough vs. multiple effects (X^2-test, p=0.057). Comparing the DSU+PSU+MU totals for M1 vs. PM, however, did confirm that the frequencies of single peak vs. single trough vs. multiple effects differed in the two cortical areas (X^2 test, p=2.85e-05), with troughs and multiple effects being more frequent in M1 and peaks more frequent in PM.

Region	Unit Quality	1 peak	1 trough	Multiple	Total
M1	DSU	1	5	7	**13**
	PSU	2	23	9	**34**
	MU	2	43	37	**82**
	Total	**5**	**71**	**53**	**129**
PM	DSU	3	0	1	**4**
	PSU	6	9	4	**19**
	MU	1	25	21	**57**
	Total	**11**	**34**	**26**	**80**
M1 + PM	DSU	4	5	8	**17**
	PSU	8	32	13	**53**
	MU	13	68	58	**139**
	Total	**25**	**105**	**79**	**209**

Table 1: Types of direct modulation. *M1 – primary motor cortex, PM – premotor cortex, DSU – definite single unit, PSU – probable single unit, MU – multi-unit*

Latency, full-width half-maximum, and amplitude of direct modulation effects in M1 and PM neurons

We then quantified the latency, full-width at half maximum, and amplitude of each peak or trough. Fig. 2A shows the distributions of peak (left) and trough (right) latencies in M1 (top row) and PM (bottom row). Although the median latency of troughs was not different in M1 versus PM (1.6 ms in M1 vs. 1.5 ms in PM, p=0.42, Mann-Whitney U-Test), the median latency of peaks was longer in M1 than in PM (4.3 ms in M1 vs. 3.4 ms in PM, p=0.04, Mann-Whitney U-Test). Inspection of the distributions shows that this difference was not due to fewer short-latency peaks produced in M1, but rather due to more peaks at longer latencies (>4ms) – an unexpected finding given that M1 is physically closer than PM to S1.

We quantified the duration of each peak or trough by measuring its full-width at half maximum (FWHM). The distributions of FWHMs (Fig. 2B) show that virtually all peaks and many troughs in both M1 and PM were relatively short-lived, with FWHMs <1 ms. In contrast to peaks, though, many troughs had FWHMs >1 ms, making the median duration of troughs longer than that of peaks in both areas (1.0 ms vs. 0.4 ms in M1, p=6.9e-07, Mann-Whitney U-Test; 0.7 ms vs 0.4 ms in PM, p=2.2e-05, Mann-Whitney U-Test). Between M1 and PM, no differences were found in FWHM for either peaks (p=0.34, Mann-Whitney U-test) or troughs (p=0.17, Mann-Whitney U-test).

We quantified the amplitudes of peaks/troughs as the maximal/minimal value expressed as a percent change from the baseline. Distributions are shown in Fig. 2C. Peak amplitudes were as high as 869% in one M1 neuron and 2650% in one PM neuron (corresponding to the probability of a spike in the peak bin of 2.5e-03 and 7.5e-03, respectively). The median percent increase for peaks was significantly higher in PM than in M1 (320% in PM vs 160% in M1, p=0.009, Mann-Whitney U-Test).

Our ability to assess trough amplitude was constrained by the spike probability floor of zero, which was reached by most troughs, resulting in a median percent decrease of 100% for both areas. We recalculated the median percent decrease after excluding values of 100%. The median percent decrease of the remaining troughs was still substantial in both areas: 90% for M1 and 80% for PM.

The relatively short latency of some peaks raised the possibility that S1-ICMS might have excited some neurons in M1 or PM antidromically. Antidromic responses would be expected to produce very narrow peaks with cumulative probabilities approaching 1.0, reflecting one-to-one following. However, antidromic responses evoked by stimulation of thin, unmyelinated axon collaterals may not follow stimulation at frequencies ~100 Hz, with as few as 10% of stimulus pulses evoking a somatic action potential (Chomiak and Hu, 2007). In Fig. 3A we have plotted the FWHM of each peak we evoked with S1-ICMS against its cumulative probability. Most peaks had cumulative probabilities <0.05. Of the

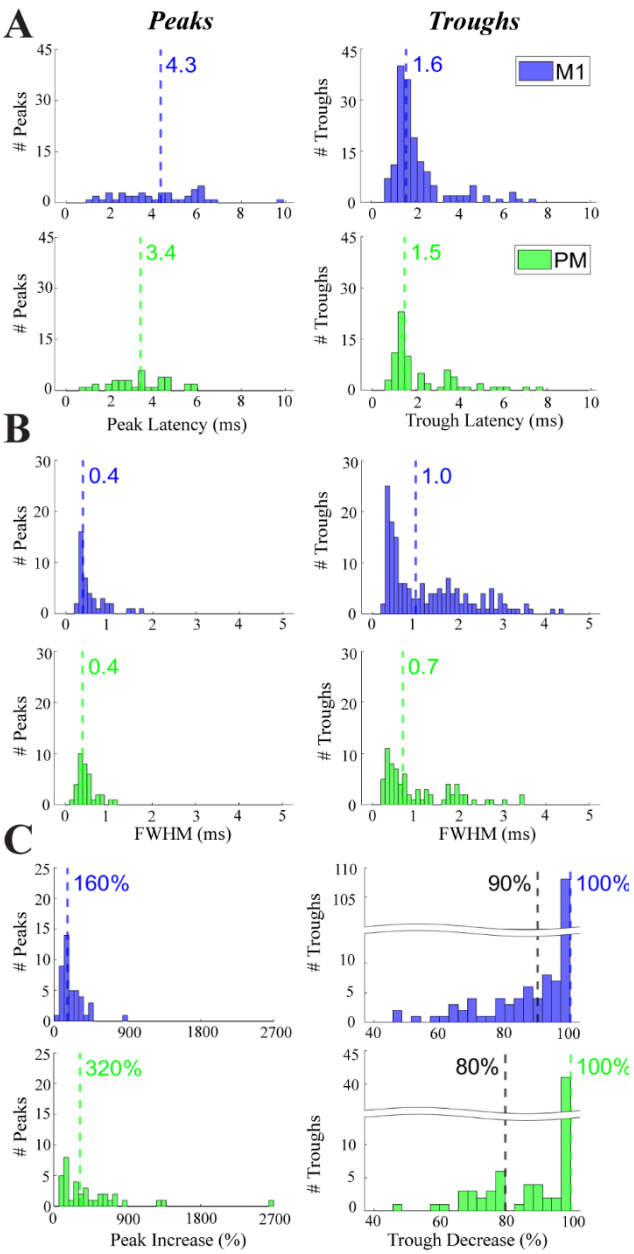

Figure 2. Properties of excitatory and inhibitory effects observed in M1 (blue) and PM (green) neurons following S1-ICMS pulses. *Separate histograms are shown for peaks (left column) and troughs (right column). Dashed vertical lines mark the median of each distribution.* ***A)*** *Latencies. The range of latencies was similar for excitation and inhibition in both M1 and PM, though short-latency troughs were more common than short-latency peaks in both areas. Histogram bin size is 0.3 ms.* ***B)*** *Full-Width Half-Maxima (FWHM). Most peaks and troughs in both M1 and PM were of relatively short duration, though some troughs lasted longer than any peaks. Histogram bin size is 0.1 ms.* ***C)*** *Amplitude (percent change from baseline). Black dashed lines mark medians after excluding all values of 100%, the floor for inhibition of 0 spikes. Histogram bin size is 60% for peaks and 3% for troughs.*

few with cumulative probabilities >0.05, an M1 neuron had the narrowest FHWM (arrow). The PSTH with this peak is shown above in Fig. 1C. Fig. 3B illustrates the jitter of the first action potentials of this M1 unit following 10 stimulus artifacts, indicating that excitation of this M1 neuron was orthodromic and transsynaptic. We thus infer that most, if not all, of the peaks we found represented orthodromic, transsynaptic excitation.

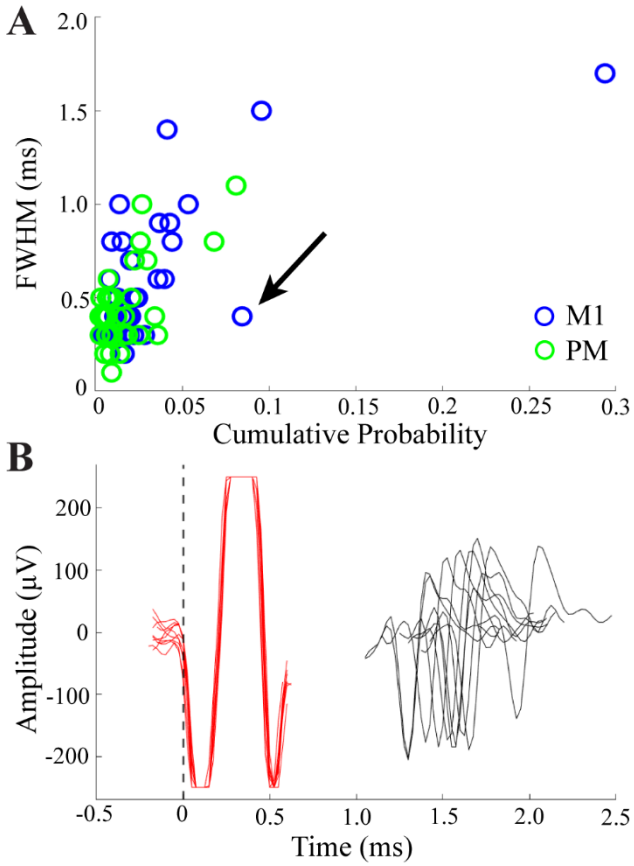

Figure 3. Cumulative probability vs. FWHM and Jitter of S1-ICMS effects. A) *Cumulative probability versus full-width half-maximum of each peak from M1 (blue) and PM (green). Cumulative probabilities were calculated by summing each bin in the PSTH from the onset of the peak to the offset (described in the Methods, Fig. 9). The black arrow indicates a point that represents a peak with both a relatively high cumulative probability and a narrow FWHM, as might be expected of an antidromic response.* ***B)*** *Overlay of 10 ICMS pulse artifacts (red traces) and the 10 following spikes (black traces) from the neuron-array pair denoted by the black arrow in* ***A****. Both waveforms were triggered on the timestamp of the assigned ICMS artifacts from the designated artifact channel described in Methods (0 ms, vertical dashed line). The jitter in the latencies of the spike waveforms relative to the artifact waveforms indicates orthodromic, transsynaptic excitation. The PSTH of this neuron-array pair is shown in Figure 1C.*

<u>Spatial convergence and divergence of S1-ICMS effects on neurons across M1 and PM</u>

Next, we examined the spatial convergence of effects from multiple S1 arrays onto individual units in M1 and PM, as well as the spatial divergence of effects from stimulation of each S1 array to units across each cortical area. We present our findings on convergence and divergence in both tabular (Fig. 4) and graphic (Fig. 5) form.

In both monkeys, ICMS effects from multiple different S1 arrays converged on individual neurons in both M1 and PM. Figure 4 (Convergence, left) gives the percentage of neurons recorded on each array in M1 or PM that had at least one significant peak or trough following ICMS delivered through different numbers of arrays in S1. Focusing on the right column (4) in monkey L, for example, shows that ICMS effects converged from all four S1 arrays on some individual units recorded from each of the four M1 arrays and from one of the four PM arrays. In monkey X, ICMS effects from converged from all three S1 arrays on individual units from two of the four M1 arrays and from one of the two PM arrays. In total, 13/38 (34%) M1 units and 1/42 (2%) PM units received effects converging from all four S1 arrays in monkey L, and 3/36 (8%) M1 and 1/33 (3%) PM units received effects converging from all three S1 arrays in monkey X. In each monkey, other units received effects converging from fewer S1 arrays as well. ICMS effects from wide territories in S1 thus converged on many neurons in both M1 and PM.

Conversely, ICMS effects from each S1 array diverged to neurons recorded on multiple different arrays in both M1 and PM. Figure 4 (Divergence, right) gives the percentage of neurons recorded on each M1 or PM array that had at least one peak or trough following ICMS pulses delivered through each S1 array. Looking down the columns shows that in monkey L, ICMS effects diverged to neurons on all 4 M1 arrays from each of the 4 S1 arrays, and diverged to all 4 PM arrays from 2 of the 4 S1 arrays (M and N). In

M1
PM

Convergence

Monkey L

# Units	Array	# S1 Arrays Producing Peak/Trough: 0	1	2	3	4
11	G	18%	36%	18%	0%	27%
5	I	0%	80%	0%	0%	20%
8	J	0%	14%	29%	29%	29%
15	K	20%	13%	7%	13%	47%
9	A	67%	11%	22%	0%	0%
7	B	57%	29%	14%	0%	0%
12	C	17%	42%	17%	25%	0%
13	D	31%	38%	15%	8%	8%

M1 vs. PM: p=0.002, χ^2-test

Monkey X

# Units	Array	# S1 Arrays Producing Peak/Trough: 0	1	2	3
5	F	0%	60%	20%	20%
11	G	18%	55%	27%	0%
2	H	0%	0%	0%	100%
18	I	33%	33%	33%	0%
12	C	8%	83%	0%	8%
18	D	17%	61%	22%	0%

M1 vs. PM: p=0.14, χ^2-test

Divergence

Monkey L

# Units	Array	S1-ICMS Arrays: M	N	O	P
11	G	73%	27%	55%	27%
5	I	20%	80%	40%	20%
8	J	71%	71%	43%	86%
15	K	67%	60%	73%	53%
9	A	33%	11%	0%	11%
7	B	29%	29%	0%	0%
12	C	50%	67%	17%	17%
13	D	31%	38%	23%	31%

M1 vs. PM: p=1.0e-7, χ^2-test

Monkey X

# Units	Array	S1-ICMS Arrays: K	L	O
5	F	60%	40%	60%
11	G	73%	18%	18%
2	H	100%	100%	100%
18	I	50%	50%	0%
12	C	92%	8%	8%
18	D	78%	17%	11%

M1 vs. PM: p=0.25 χ^2-test

***Figure** 4. **S1-ICMS effects by array.** For convergence tables (left), each entry gives the percent of units on each M1 (blue) or PM (green) array that had a significant peak and/or trough in the PSTHs triggered on artifacts of ICMS pulses delivered through different numbers of S1 arrays, from 0 to 4. For divergence tables (right), each entry gives the percent of units on each M1 or PM array with a peak and/or trough in the PSTH triggered on artifacts from ICMS pulses delivered through the indicated S1 array. All entries are color coded on a scale from white (0%) to dark blue/green (100%, M1/PM). Results for monkey L are displayed above and results for monkey X below.*

monkey X, ICMS effects diverged to neurons on all 4 M1 arrays from 2 of the 3 S1 arrays (K and L), and diverged to neurons from both PM arrays from all three S1 arrays.

We then compared the convergence and divergence of S1-ICMS effects between M1 and PM. By comparing counts of units receiving direct modulation from 0, 1, 2, 3, or 4 S1 arrays, we found that in both monkeys individual M1 units were directly modulated by ICMS delivered on more S1 arrays

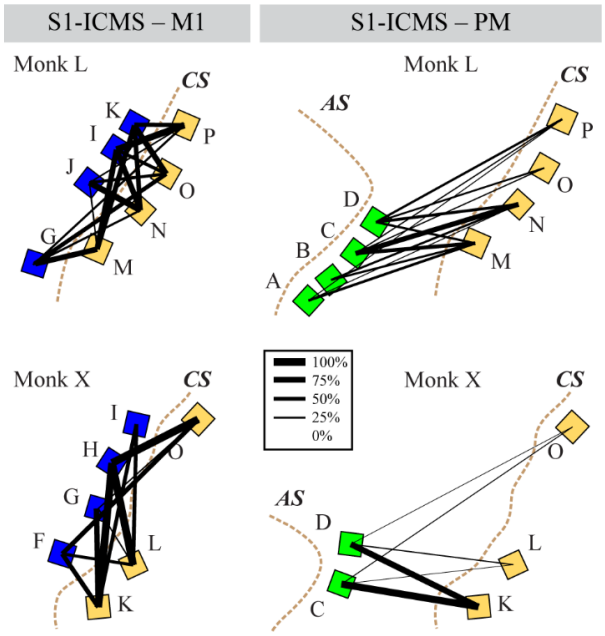

Figure 5. Graphic topography of direct modulation effects from each S1 array. *Each square represents an FMA implanted in PM (green), M1 (blue) or S1 (yellow). The thickness of each solid black line is proportional to the percentage of units recorded from each M1 or PM array that showed a peak and/or trough following ICMS pulses delivered through the connected S1 array. The letters next to the arrays correspond to those in Figure 4. Brown dotted lines indicate sulci: Arcuate Sulcus (AS) and Central Sulcus (CS).*

than were individual PM units. This trend was significant in monkey L (p=0.002, χ^2 test), though not in monkey X (p=0.14, χ^2 test). We also found that in both monkeys S1-ICMS delivered on individual arrays diverged to modulate units across M1 more commonly than PM, though again this trend was significant in monkey L (p=1.0e-7, χ^2 test), but not in monkey X (p=0.25, χ^2 test). As illustrated by the thickness of the black lines in Figure 5, both convergence and divergence of ICMS effects were more extensive from S1 to M1 than from S1 to PM.

Discussion

We found that ICMS pulses delivered in S1 as instructions during a reach-grasp-manipulate task directly modulated the spiking activity of a majority of neurons recorded in two other cortical regions, M1 and PM. Although one of our PM arrays in monkey X may have been in the dorsal premotor cortex, the remainder in both monkeys were in the ventral premotor cortex (PMv). For purposes of the present discussion, we therefore will refer to PMv. In both M1 and PMv, we found inhibitory effects to be more common than excitatory effects. In addition, the duration of inhibitory effects was often longer than that of excitatory effects. S1 outputs thus may produce more inhibition than excitation in both M1 and PMv.

We also found extensive divergence of effects from S1 to both M1 and PMv. ICMS pulses delivered simultaneously via a few electrodes on a single ~2x2 mm array in S1 produced effects in neurons recorded on other ~2x2 mm microelectrode arrays spread throughout the upper extremity representation in M1 and over a considerable territory in PMv. Conversely, many single- or multi-units anywhere in these regions of M1 and PM received effects converging from all arrays spread across the S1 upper extremity representation. Although macaque S1 has a detailed somatotopic organization (Pons et al., 1985; Pons et al., 1987), its outputs to M1 and PMv appear to have less somatotopic segregation.

Physiological and anatomical bases of distant effects produced by S1-ICMS

In macaque and cebus monkeys, neurons in both M1 and PMv are known to receive somatosensory input. In M1, neurons respond to both cutaneous and deep peripheral stimulation (Fetz et al., 1980; Lemon and Porter, 1976; Rosen and Asanuma, 1972; Wong et al., 1978). In PMv, neurons also respond to both cutaneous and deep peripheral stimulation, but have larger and more complex somatosensory receptive fields (Graziano and Gandhi, 2000; Rizzolatti et al., 1981). Consistent with this natural sensory input, we found that more than 60% of single- and multi-units in M1 and PMv were directly modulated by ICMS pulses delivered through at least one S1 microelectrode array.

The pathways via which natural somatosensory input reaches M1 and PMv are not entirely understood, though a substantial fraction may be processed through S1. We were not able to obtain histological verification of the locations of our microelectrode tips, but based on the distance of our S1 arrays from the central sulcus (<3 mm) and their lengths (1.5 – 6.0 mm), the tips of our S1 electrodes were probably located in areas 3b and 1, with some possibly in area 3a. Area 3a projects directly to M1 (area 4), but areas 3a, 3b and 1 all project to area 2, which in turn projects to area 4 (Dariansmith et al., 1993; Jones et al., 1978; Padberg et al., 2019; Pons and Kaas, 1986; Tokuno and Tanji, 1993). Area 2 also projects to area 5, which projects more heavily to area 4 (Strick and Kim, 1978; Zarzecki et al., 1978). All of these parietal areas also project to the secondary somatosensory area (S2) in the insular cortex, which in turn projects to area 4 (Dariansmith et al., 1993; Friedman et al., 1986). Whereas multiple transsynaptic routes are available from S1 to M1, routes from S1 to PMv are more limited. Known somatosensory projections to PMv arise only from area 3a and from S2 (Godschalk et al., 1984; Kurata, 1991; Matelli et al., 1986). The greater variety of transsynaptic routes from S1 to M1 may account in part for the distribution of

latencies for peaks in M1 being slightly wider, with a slightly longer median latency compared to PMv (Fig. 2A).

The latencies and durations we observed in the present study were consistent with those observed in other studies following natural and electrical stimulation of peripheral and cortical neurons. The latencies of M1 responses to natural stimulation of the upper extremity or electrical stimulation of the median nerve range from 8 to 15 ms (Lemon, 1981). As would be expected, we found the latencies of effects produced in M1 by ICMS pulses delivered in S1 (0.9 – 9.9 ms for peaks, 0.6 – 7.2 ms for troughs) to be shorter than peripheral latencies. Although our S1-ICMS pulses were delivered at frequencies of ~100 Hz, the latencies we observed in M1 neurons were in the same range as those found in M1 in a study using PMv-ICMS pulses delivered at 10 Hz (1.8 –3.0 ms for peaks, 2–5 ms for troughs) (Kraskov et al., 2011). In humans, S1-ICMS at 100 Hz produced effects in M1 neurons at similar latencies (2–6 ms) (Shelchkova et al., 2022). Moreover, the durations of the S1-ICMS effects we found in M1 (FWHMs 0.2 – 1.7 ms for peaks, 0.3 – 4.3 ms for troughs), were similar to those obtained with PMv-ICMS (durations ~1ms for peaks, 5–7 ms for troughs).

A surprising observation was that the range of latencies we found for excitatory peaks in PMv neurons (0.6 – 5.8 ms) was somewhat shorter than for those in M1 neurons (0.9 – 9.9 ms), even though the physical distance from S1 to PMv is longer than from M1 to S1. Though the present latencies in PMv neurons might seem unexpectedly short, they are similar to the range reported from area 5 to M1 (0.9 – 4.4 ms) (Zarzecki et al., 1978), which covers a similar physical distance. These observations may indicate that conduction velocities are faster from S1 to PMv than to M1. In addition, the longer latencies of some effects in M1 neurons from S1-ICMS may reflect the presence of more diverse transsynaptic routes from S1 to M1 than to PMv.

We consider it unlikely that the peaks we identified represented antidromic conduction. To our knowledge, there is no evidence that PM projects directly to S1. For M1, antidromic responses would be unlikely because axons from area 4, though projecting to areas 3a and 2, do not project to areas 3b or 1 (Dariansmith et al., 1993; Godschalk et al., 1984; Matelli et al., 1986), where most of our electrode tips probably were situated. Furthermore, for the neuron-array pair having a peak with both a high cumulative spike probability and a narrow FWHM, the first spike following the stimulus artifact showed temporal jitter consistent with orthodromic conduction and transsynaptic excitation. Therefore, the direct effects S1-ICMS evoked in M1 and PM neurons in this study were most likely orthodromic.

Implications of the diverse properties of distant S1-ICMS effects

Another property of the distant effects observed here was that S1-ICMS produced more inhibition than excitation in both M1 and PMv. Somatosensory inputs have been typically assessed by determining the receptive fields from which neurons in S1, M1, or PMv can be excited. We therefore had not anticipated that S1-ICMS would produce both more frequent and longer duration inhibitory effects than excitatory effects in both M1 and PMv neurons. We were able to detect this inhibitory modulation because we delivered S1-ICMS during the reaction and movement epochs of a behavioral task during which M1 and PMv neurons were active. PMv-ICMS also has been delivered during active movements but, in contrast to the present results, produced more excitatory than inhibitory modulation of M1 neurons (Kraskov et al., 2011). We suggest that during active movements, while PMv generally facilitates activity in M1, S1 may provide inhibition of undesired activity in both M1 and PMv, acting to focus motor activity on the desired movement.

We also observed extensive convergence and divergence between our arrays that spanned the upper extremity representation in S1 and our arrays in both M1 and PMv. This might have been expected in

PMv given the large somatosensory receptive fields of PMv neurons (Graziano and Gandhi, 2000; Rizzolatti et al., 1981). Less expected perhaps, was the similarly extensive convergence and divergence between our S1 arrays and those in M1, which spanned the M1 upper extremity representation. A recent study in humans likewise found that ICMS on many S1 electrodes evoked responses in M1 neurons, mostly consistent with orthodromic, transsynaptic responses (Shelchkova et al., 2022). Interestingly, focal injection of tracers in area 3a, 3b, 1, or 2 results in terminal labeling spread mediolaterally over several millimeters in the same cortical area (Jones et al., 1978). Likewise neurons at any focal location in the M1 upper extremity representation send horizontal collaterals throughout that representation (Huntley and Jones, 1991). Horizontal collaterals in both S1 and M1 thus may provide an anatomical substrate for the convergence and divergence we observed physiologically between S1 and M1.

Whereas previous studies typically have delivered ICMS through a single microelectrode, the present results are based on ICMS pulses delivered simultaneously through multiple microelectrodes on the same ~2x2 mm array. We chose to deliver ICMS in this manner to make it more likely that our monkeys would perceive some component of the multi-electrode S1-ICMS and thereby be able to use it as an instruction (Mazurek and Schieber, 2017). Interestingly, recent studies of human S1 have reported that stimulating simultaneously through multiple microelectrodes may be a useful approach for evoking artificial sensations. Multi-channel S1-ICMS evokes tactile sensations more focal (Greenspon et al., 2023a), at shorter latencies (Bjanes et al., 2022; Sombeck and Miller, 2019), and with more distinguishable levels of perceived force (Greenspon et al., 2023b) than stimulating through a single microelectrode. Multi-electrode ICMS therefore may become a useful approach in bidirectional brain-computer interfaces (Flesher et al., 2021; O'Doherty et al., 2011). If so, then the effects of direct modulation of M1 and PM neurons produced by multi-electrode S1-ICMS like that used here will need to be taken into account in decoding the intended movement from neural activity in these cortical motor areas.

Acknowledgements

The authors thank Gil Rivlis for custom task-control and stimulation control software, and Marsha Hayles for editorial comments.

Author contributions

BR, KAM and MHS designed the study. KAM collected and processed the data and performed some preliminary analyses. BR performed the analyses and wrote the manuscript. MHS supervised, provided resources, and edited the manuscript.

Declaration of interests

The authors declare no competing financial interests.

Funding sources

This work was supported by grants F31NS129099 (BR), F32NS093709 (KAM), and R01NS107271 (MHS) from the National Institute of Neurological Disorders and Stroke. The funders had no role in study design, data collection or interpretation, nor in the decision to submit the work for publication.

References

Andersen, P., Hagan, P.J., Phillips, C.G., and Powell, T.P. (1975). Mapping by microstimulation of overlapping projections from area 4 to motor units of the baboon's hand. Proc R Soc Lond B Biol Sci 188, 31-36.

Asanuma, H., and Ward, J.E. (1971). Patterns of contraction of distal forelimb muscles produced by intracortical stimulation in cats. Brain Res 27, 97-109.

Bjanes, D.A., Bashford, L., Pejsa, K., Lee, B., Liu, C.Y., and Andersen, R.A. (2022). Multi-channel intra-cortical micro-stimulation yields quick reaction times and evokes natural somatosensations in a human participant. medRxiv.

Chomiak, T., and Hu, B. (2007). Axonal and somatic filtering of antidromically evoked cortical excitation by simulated deep brain stimulation in rat brain. J Physiol 579, 403-412.

Dariansmith, C., Dariansmith, I., Burman, K., and Ratcliffe, N. (1993). Ipsilateral Cortical Projections to Area-3a, Area-3b, and Area-4 in the Macaque Monkey. Journal of Comparative Neurology 335, 200-213.

Fetz, E.E., Finocchio, D.V., Baker, M.A., and Soso, M.J. (1980). Sensory and motor responses of precentral cortex cells during comparable passive and active joint movements. Journal of Neurophysiology 43, 1070-1089.

Flesher, S.N., Downey, J.E., Weiss, J.M., Hughes, C.L., Herrera, A.J., Tyler-Kabara, E.C., Boninger, M.L., Collinger, J.L., and Gaunt, R.A. (2021). A brain-computer interface that evokes tactile sensations improves robotic arm control. Science (American Association for the Advancement of Science) 372, 831-836.

Fraser, G.W., and Schwartz, A.B. (2012). Recording from the same neurons chronically in motor cortex. Journal of neurophysiology 107, 1970-1978.

Friedman, D.P., Murray, E.A., Oneill, J.B., and Mishkin, M. (1986). Cortical Connections of the Somatosensory Fields of the Lateral Sulcus of Macaques - Evidence for a Corticolimbic Pathway for Touch. Journal of Comparative Neurology 252, 323-347.

Gentilucci, M., Fogassi, L., Luppino, G., Matelli, M., Camarda, R., and Rizzolatti, G. (1988). Functional organization of inferior area 6 in the macaque monkey. I. Somatotopy and the control of proximal movements. ExpBrain Res 71, 475-490.

Godschalk, M., Lemon, R.N., Kuypers, H.G., and Ronday, H.K. (1984). Cortical afferents and efferents of monkey postarcuate area: an anatomical and electrophysiological study. Exp Brain Res 56, 410-424.

Graziano, M.S., and Gandhi, S. (2000). Location of the polysensory zone in the precentral gyrus of anesthetized monkeys. ExpBrain Res 135, 259-266.

Greenspon, C.M., Shelchkova, N.D., Valle, G., Hobbs, T.G., Berger-Wolf, E.I., Hutchinson, B.C., Dogruoz, E., Verbaarschot, C., Callier, T., Sobinov, A.R., *et al.* (2023a). Tesslation of artificial touch via microstimulation of human somatosensory cortex. bioRxiv.

Greenspon, C.M., Valle, G., Hobbs, T.G., Verbaarschot, C., Callier, T., Okorokova, E.V., Shelchkova, N.D., Sobinov, A.R., Jordan, P.M., Gonzalez-Martinez, J., *et al.* (2023b). Biomimetic multi-channel microstimulation of somatosensory cortex conveys high resolution force feedback for bionic hands. Neuroscience.

Guggenmos, D.J., Azin, M., Barbay, S., Mahnken, J.D., Dunham, C., Mohseni, P., and Nudo, R.J. (2013). Restoration of function after brain damage using a neural prosthesis. Proceedings of the National Academy of Sciences - PNAS 110, 21177-21182.

Histed, M.H., Bonin, V., and Reid, R.C. (2009). Direct Activation of Sparse, Distributed Populations of Cortical Neurons by Electrical Microstimulation. Neuron (Cambridge, Mass) 63, 508-522.

Huntley, G.W., and Jones, E.G. (1991). Relationship of intrinsic connections to forelimb movement representations in monkey motor cortex: a correlative anatomic and physiological study. Journal of Neurophysiology 66, 390-413.

Hussin, A.T., Boychuk, J.A., Brown, A.R., Pittman, Q.J., and Teskey, G.C. (2015). Intracortical Microstimulation (ICMS) Activates Motor Cortex Layer 5 Pyramidal Neurons Mainly Transsynaptically. Brain stimulation 8, 742-750.

Jankowska, E., Padel, Y., and Tanaka, R. (1975). The mode of activation of pyramidal tract cells by intracortical stimuli. J Physiol 249, 617-636.

Jones, E.G., Coulter, J.D., and Hendry, S.H. (1978). Intracortical connectivity of architectonic fields in the somatic sensory, motor and parietal cortex of monkeys. J Comp Neurol 181, 291-347.

Kraskov, A., Prabhu, G., Quallo, M.M., Lemon, R.N., and Brochier, T. (2011). Ventral premotor-motor cortex interactions in the macaque monkey during grasp: response of single neurons to intracortical microstimulation. J Neurosci 31, 8812-8821.

Kurata, K. (1991). Corticocortical inputs to the dorsal and ventral aspects of the premotor cortex of macaque monkeys. Neuroscience Research 12, 263-280.

Lemon, R.N. (1981). Functional properties of monkey motor cortex neurones receiving afferent input from the hand and fingers. Journal of Physiology - London 311, 497-519.

Lemon, R.N., and Porter, R. (1976). Afferent input to movement-related precentral neurones in conscious monkeys. ProcRSocLond 194, 313-339.

Maier, M.A., Kirkwood, P.A., Brochier, T., and Lemon, R.N. (2013). Responses of single corticospinal neurons to intracortical stimulation of primary motor and premotor cortex in the anesthetized macaque monkey. J Neurophysiol 109, 2982-2998.

Matelli, M., Camarda, R., Glickstein, M., and Rizzolatti, G. (1986). Afferent and efferent projections of the inferior area 6 in the macaque monkey. JComp Neurol 251, 281-298.

Mazurek, K.A., and Schieber, M.H. (2017). Injecting Instructions into Premotor Cortex. Neuron 96, 1282-1289 e1284.

Mazurek, K.A., and Schieber, M.H. (2019). How is electrical stimulation of the brain experienced, and how can we tell? Selected considerations on sensorimotor function and speech. Cogn Neuropsychol 36, 103-116.

Mazurek, K.A., and Schieber, M.H. (2021). Injecting Information into the Mammalian Cortex: Progress, Challenges, and Promise. The Neuroscientist 27, 129-142.

Mollazadeh, M., Aggarwal, V., Davidson, A.G., Law, A.J., Thakor, N.V., and Schieber, M.H. (2011). Spatiotemporal variation of multiple neurophysiological signals in the primary motor cortex during dexterous reach-to-grasp movements. J Neurosci 31, 15531-15543.

O'Doherty, J.E., Lebedev, M.A., Ifft, P.J., Zhuang, K.Z., Shokur, S., Bleuler, H., and Nicolelis, M.A.L. (2011). Active tactile exploration using a brain-machine-brain interface. Nature (London) 479, 228-231.

Padberg, J., Cooke, D.F., Cerkevich, C.M., Kaas, J.H., and Krubitzer, L. (2019). Cortical connections of area 2 and posterior parietal area 5 in macaque monkeys. J Comp Neurol 527, 718-737.

Pandarinath, C., and Bensmaia, S.J. (2022). The science and engineering behind sensitized brain-controlled bionic hands. Physiol Rev 102, 551-604.

Pons, T.P., Garraghty, P.E., Cusick, C.G., and Kaas, J.H. (1985). The somatotopic organization of area 2 in macaque monkeys. Journal of Comparative Neurology 241, 445-466.

Pons, T.P., and Kaas, J.H. (1986). Corticocortical connections of area 2 of somatosensory cortex in macaque monkeys: a correlative anatomical and electrophysiological study. J Comp Neurol 248, 313-335.

Pons, T.P., Wall, J.T., Garraghty, P.E., Cusick, C.G., and Kaas, J.H. (1987). Consistent features of the representation of the hand in area 3b of macaque monkeys. Somatosensory Research 4, 309-331.

Rizzolatti, G., Camarda, R., Fogassi, L., Gentilucci, M., Luppino, G., and Matelli, M. (1988). Functional organization of inferior area 6 in the macaque monkey. II. Area F5 and the control of distal movements. ExpBrain Res 71, 491-507.

Rizzolatti, G., Scandolara, C., Matelli, M., and Gentilucci, M. (1981). Afferent properties of periarcuate neurons in macaque monkeys. I. Somatosensory responses. Behavioural Brain Research 2, 125-146.

Rosen, I., and Asanuma, H. (1972). Peripheral afferent inputs to the forelimb area of the monkey motor cortex: input-output relations. Experimental Brain Research 14, 257-273.

Rouse, A.G., and Schieber, M.H. (2016). Spatiotemporal distribution of location and object effects in primary motor cortex neurons during reach-to-grasp. The Journal of neuroscience 36, 10640-10653.

Shelchkova, N.D., Downey, J.E., Greenspon, C.M., Okorokova, E.V., Sobinov, A.R., Verbaarschot, C., He, Q., Sponheim, C., Totolani, A.F., Moore, D.D., *et al.* (2022). Microstimulation of human somatosensory cortex evokes taskdependent, spatially patterned responses in motor cortex. bioRxiv.

Sombeck, J.T., and Miller, L.E. (2019). Short reaction times in response to multi-electrode intracortical microstimulation may provide a basis for rapid movement-related feedback. J Neural Eng 17, 016013.

Stoney, S.D., Jr., Thompson, W.D., and Asanuma, H. (1968). Excitation of pyramidal tract cells by intracortical microstimulation: effective extent of stimulating current. J Neurophysiol 31, 659-669.

Strick, P.L., and Kim, C.C. (1978). Input to primate motor cortex from posterior parietal cortex (area 5). I. Demonstration by retrograde transport. Brain Res 157, 325-330.

Tokuno, H., and Tanji, J. (1993). Input organization of distal and proximal forelimb areas in the monkey primary motor cortex: a retrograde double labeling study. Journal of Comparative Neurology 333, 199-209.

Wong, Y.C., Kwan, H.C., MacKay, W.A., and Murphy, J.T. (1978). Spatial organization of precentral cortex in awake primates. I. Somatosensory inputs. Journal of neurophysiology 41, 1107-1119.

Zarzecki, P., Strick, P.L., and Asanuma, H. (1978). Input to primate motor cortex from posterior parietal cortex (area 5). II. Identification by antidromic activation. Brain Res 157, 331-335.

STAR Methods

CONTACT FOR REAGENT AND RESOURCE SHARING

Further information and requests for resources and reagents should be directed to and will be fulfilled by the Lead Contact, Marc H. Schieber (mschiebe@ur.rochester.edu).

EXPERIMENTAL MODEL AND SUBJECT DETAILS

Non-human primates. Two male rhesus monkeys (Monkeys L and X, weight 9 and 11 kg, age 11 and 13 years old, respectively) were subjects in the present study. All procedures for the care and use of these nonhuman primates followed the Guide for the Care and Use of Laboratory Animals and were approved by the University Committee on Animal Resources at the University of Rochester, Rochester, New York.

METHOD DETAILS

Methods used for behavioral training, neural recording, and delivering ICMS, all have been described in detail previously (Mazurek and Schieber, 2017) and are summarized here only briefly.

Initial Behavioral Training for the Reach-Grasp-Manipulate Task with LED cues

Each monkey was initially trained to perform a reach-grasp-manipulate (RGM) task as described in detail previously (Mazurek and Schieber, 2017; Mollazadeh et al., 2011). The monkey initiated each trial by reaching to a central home object, grasping it, and pulling it for a variable initial hold period (700-1500 ms). Then the monkey was instructed to reach to, grasp, and manipulate 1 of 4 peripheral objects by illumination of a ring of blue LEDs around the base of that object. The 4 objects were arranged at 45º intervals 13 cm radially from the home object. The monkey pushed a button, turned a sphere, pulled a coaxial cylinder (coax), or pulled a perpendicular cylinder (perp). The monkey then held the object in the manipulated position for a final hold period of 700-1000 ms. Three hundred milliseconds after the successful completion of a trial, a water reward was delivered and the trial ended. A 1000 ms inter-trial interval occurred before another trial could be initiated. Trials for each target object were presented pseudo-randomly in blocks. Each block included one trial for each target object, and the order of the 4 instructed objects within a block was re-randomized between blocks. Errors occurred if the monkey failed to hold the home object for the required duration, failed to release the home object within 1000 ms of the instruction onset, contacted the wrong target object, failed to contact a peripheral object within 1000 ms of releasing the center object, or failed to hold the target object for the required duration. When an error occurred, trials were aborted immediately, no reward was given, and the same object was instructed again on the next trial to prevent the monkey from avoiding trials involving a particular peripheral object. Trials following an error were excluded from analysis because the monkey could have known which object would be instructed. The RGM task was controlled by a custom software written in TEMPO (Reflective Computing, Olympia, WA).

Neural Recordings

Once trained to perform the RGM task instructed with visual cues, each monkey was implanted with multiple floating microelectrode arrays (FMAs, Microprobes for Life Sciences, Gaithersburg, MD) in the primary somatosensory cortex (S1), primary motor cortex (M1), and premotor cortex (PM) of the left hemisphere, as described previously (Mollazadeh et al., 2011) (Fig. 6). Each of these cortical areas was implanted with four 16-electrode FMAs (impedance ~0.5MΩ, 70% Pt, 30% Ir). In monkey L, all 4 PM FMAs were located in the ventral premotor cortex, while in monkey X, only 2 of the 4 PM FMAs functioned well and the more medial array may have been in the dorsal premotor cortex. The intracortical location of electrode tips was confirmed by the presence of local field potentials and single- or multi-unit activity. Neural data were recorded with a Multi Acquistion Processor and SortClient software (Plexon, Inc., Dallas, TX). After 1,000 – 32,000x amplification, waveforms that crossed a threshold set online by the user were sampled at 40 kHz and saved for offline sorting along with behavioral event markers generated by the TEMPO system. After off-line sorting (Plexon Offline Sorter), the signal-to-noise ratio (SNR) and the estimated percentage of inter-spike interval (ISI) violations (< 1ms) were used to classify each sorted unit as a definite single unit (SNR ≥ 3 and no ISIs < 1ms), a probable single unit (SNR ≥ 2.5 and <10% ISIs < 1ms), a multi-unit (SNR ≥ 1.5 and <90% ISIs < 1ms), or noise (SNR < 1.5 or ≥ 90% ISIs < 1ms) (Rouse and Schieber, 2016).

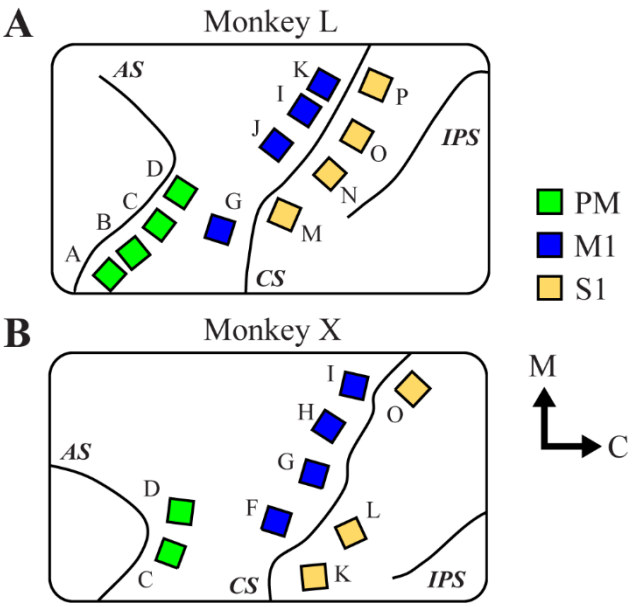

Figure 6. Location of microelectrode arrays implanted in Monkey L (A) and Monkey X (B). *Arrays (~2x2 mm) were implanted in primary motor cortex (M1, blue), premotor cortex (PM, green), and primary somatosensory cortex (S1, yellow). AS – arcuate sulcus, CS – central sulcus, and IPS – intraparietal sulcus. Letters next to each array are used to identify that array. Orientation arrows indicate medial (M) and caudal (C) directions. Modified with permission from Mazurek & Schieber,*

Learning to use ICMS instructions

Several months after the microelectrode arrays had been implanted, each monkey was trained to perform the RGM task using ICMS pulse trains delivered in S1 as instructions, instead of the visual, LED cues (Mazurek and Schieber, 2017). ICMS trains consisted of symmetric, biphasic, cathodic-leading, 200 µs per phase, 1-64 µA pulses delivered at a constant frequency. For monkey L, ICMS pulse frequency was 100 Hz for all target objects, whereas for monkey X, ICMS pulse trains had a different frequency for each object: button – 75 Hz, sphere – 100 Hz, perp – 150 Hz, coax – 225 Hz. ICMS pulses were produced by a constant-current IZ2 Neural Stimluator controlled by an RZ5 BioAmp Processor hosted by a PC running the OpenEx Software Suite (Tucker-Davis Technologies, Gainesville, FL).

Each of the 4 objects was instructed with a train of ICMS pulses delivered through electrodes on a different S1 array. Current pulses for each instruction were delivered simultaneously through a set of 3-7 electrodes all on the same S1 array. At first, these ICMS pulse trains were delivered in conjunction with the LED cues, i.e. stimulation on the S1 array assigned to the instructed target was delivered simultaneously with illumination of the LED ring surrounding that target. Then, over multiple subsequent daily sessions, the LEDs were gradually dimmed until they could remain completely off while the

monkey continued to perform well. At this point, ICMS trains served as the only instruction for the correct target object on each ICMS-instructed trial, with no visual cue.

QUANTIFICATION AND STATISTICAL ANALYSIS

All analyses presented here were performed off-line using MATLAB (MathWorks, Natick, MA),

Peristimulus Time Histograms

To determine whether M1 and PM neurons were directly modulated by pulses of S1-ICMS, we constructed four peristimulus time histograms (PSTHs) for every recorded unit – one PSTH triggered on pulse artifacts from each of the four different ICMS instructions. The time of each ICMS pulse artifact was identified offline by discriminating the waveforms of stimulation artifacts on recording channels from M1 or PM in which any spikes were much smaller than the recorded artifacts. Each rhythmic train of artifacts could be unambiguously assigned to ICMS pulses from a given S1 array based on the shapes of the four different artifact waveforms and knowledge of which object was instructed on each trial. The time window of each PSTH was chosen to span from 20% of the inter-pulse-interval before the timestamp of the triggering ICMS pulse artifact until the timestamp of the next ICMS pulse artifact. For example, a 100 Hz pulse train would have 10ms inter-pulse intervals, and therefore the PSTH window spanned from -2 ms before to +10 ms after the trigger time. A PSTH bin-width of 0.1 ms was chosen to provide high temporal resolution. Raw spike counts in each bin were divided by the total number of ICMS trigger pulses, such that the PSTH ordinate represented the probability of the neuron firing a spike in each 0.1 ms bin (Guggenmos et al., 2013). Figure 7 illustrates one of the four PSTHs (for instruction 1, the button) for a definite single unit in M1.

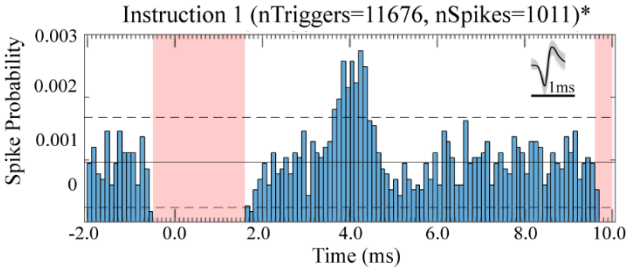

Figure 7. Example peristimulus time histogram. *Across multiple RGM trials, this definite single unit from M1 fired a total of 1011 spikes (nSpikes) during ICMS Instruction 1 (button). Spike counts in each 0.1ms bin were converted to probabilities by dividing the count in each bin by the number of ICMS pulse artifacts used as triggers to form the PSTH (nTriggers). Pink rectangles show the artifact window during which spikes could not be reliably discriminated. Horizontal black lines represent the mean (solid line) ± 2 standard deviations (dashed lines) of the baseline bins preceding the first artifact window. The average waveform of the unit is shown in the upper right corner of the PSTH, with overlapped individual spikes in gray and a 1ms timescale bar below in black. Ch78U2, L, 20150729.*

When ICMS pulse artifacts crossed the threshold set online during the recording session, neural data was blanked from -0.2ms to +0.6ms surrounding the timestamp assigned by Offline Sorter. We considered any spike waveform on an M1 or PM recording channel that occurred during this interval to have been potentially distorted by collision with an ICMS pulse artifact. Any neuron spikes occurring in this interval therefore were omitted from the PSTH, producing a minimum blanked window from -0.2 ms to +0.6 ms around the trigger time at 0.0 ms. ICMS pulse artifacts varied across different recording channels, however, often having waveforms different from the artifacts in the channels used to trigger each PSTH. In some recording channels, the artifacts could begin more than 0.2 ms before the timestamp or last longer than 0.6 ms after the timestamp. We therefore determined the duration of the full artifact window separately for each PSTH, using the 15th percentile of all the bins in each PSTH as a threshold. We defined the first bin that exceeded the 15th percentile proceeding backward from time 0.0 ms to be the start and the first bin proceeding forward from time 0.0 ms to be the end of the ICMS pulse artifact on that channel. Any spikes within this “final artifact window” (shaded pink in all PSTH figures) were excluded from subsequent analyses.

In one situation, we truncated the final artifact window earlier than the 15th percentile threshold crossing after time 0.0 ms. As illustrated by the example PSTH of Fig. 8A, the trigger time sometimes was followed by a prolonged series of bins with zero spike counts, suggesting that the ICMS pulses produced early inhibition of the unit. We therefore set a maximum duration for artifact windows to distinguish early inhibition following ICMS pulses from spikes lost due to collisions with the ICMS artifacts. To determine that maximum duration, we identified the time between the artifact onset and the earliest spike discriminated after the +0.6 ms minimum for each of the 596 constructed PSTHs. We then compiled a histogram of those earliest spike latencies (Fig. 8B), which appeared bimodal. We interpreted the first mode to represent PSTHs in which spikes occurred immediately following the ICMS pulse artifact and the second mode to represent PSTHs in which spikes resumed after a period of early inhibition. We fit a generalized Gaussian mixture model to the bimodal distribution and used the nadir between the two components at 2.1 ms as the maximum possible duration of an ICMS pulse artifact window. Any artifact window lasting longer than 2.1 ms after its onset according to the 15th percentile threshold was truncated at 2.1 ms. Whereas bins during the artifact window were excluded from subsequent analyses, a series of zero-count bins beyond 2.1 ms was considered to indicate a period of inhibition rather than collisions with artifacts and therefore was included in subsequent analyses.

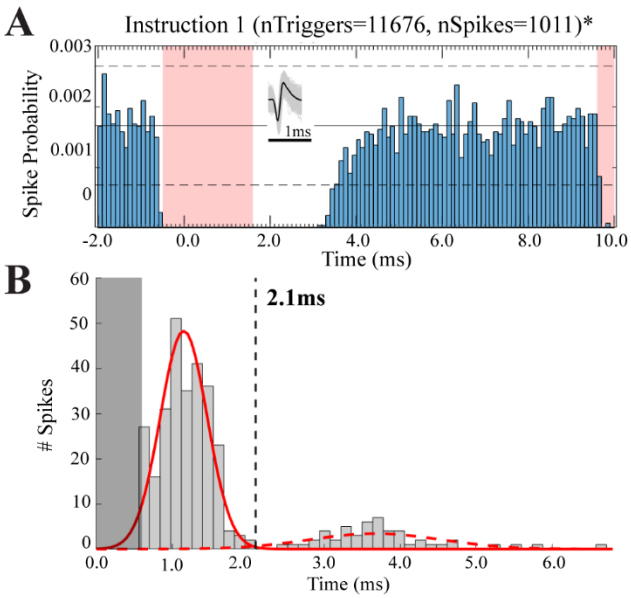

Figure 8. Distinguishing early inhibition from collisions with ICMS pulse artifacts. A) *Example PSTH in which a period of early inhibition followed the ICMS pulse artifact. The final artifact window began -0.5ms before the trigger time and ended 2.1ms later at +1.6ms.* ***(****Ch114U1, L, 20150729).* ***B)*** *For every PSTH, the earliest spike after the artifact window determined by the 15th percentile was collected and binned in 0.1ms steps. The distribution appeared bimodal, so a generalized Gaussian mixture model with two components was fit to the data. The first component was interpreted as spikes resuming as soon as the artifact ended whereas the second was interpreted as spikes resuming after an early inhibitory period immediately following the artifact. The nadir between the two components was therefore set as the maximum artifact window duration (2.1ms).*

<u>Modulation in PSTHs</u>

In the PSTH of each neuron-array pair, we identified excitatory peaks and/or inhibitory troughs when ≥3 consecutive bins went beyond ± 2 standard deviations of the baseline mean calculated from the bins preceding the final artifact window. In cases for which the mean minus 2 standard deviations was less than zero, we required 7 consecutive bins with counts of zero to identify a trough. For 59 pairs we did not attempt to identify troughs because the total spike count was <100, producing many bins that contained zero spikes by chance alone.

We then measured the latency, full width at half maximum (FWHM), and amplitude of each peak or trough, as illustrated in Figure 9. Latencies were calculated as the time from the beginning of the final artifact window to the first bin in which a peak or trough crossed above or below two standard deviations from the mean of the baseline spike probability. FWHM was calculated as the difference in time between the bins in which a peak or trough crossed 50% of its maximum or minimum value with respect to the baseline mean. We quantified amplitude as the maximum of a peak or the minimum of a trough minus the

baseline mean, normalized as a percentage of the baseline mean. For peaks, we also calculated the cumulative probability as the sum of the probability in each bin from onset to offset of the peak.

Some PSTHs appeared to show some degree of modulation although any of their peaks and/or troughs

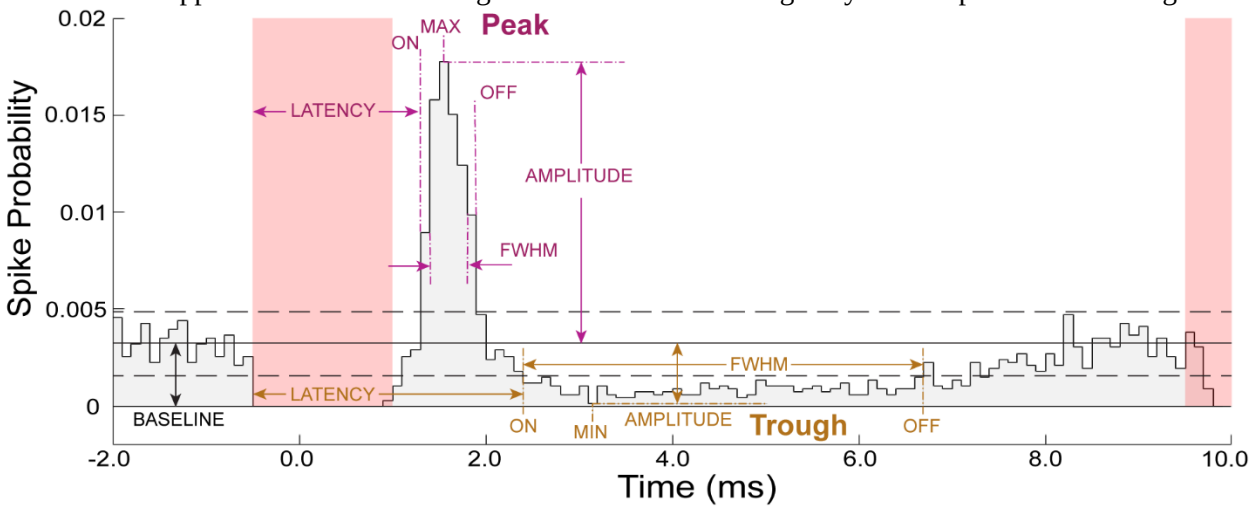

Figure 9. Peak and trough characteristics. *Peaks and troughs were identified when the PSTH crossed 2 standard deviations (horizontal dashed line) beyond the mean (horizontal solid line) of the baseline period before the final artifact window (pink rectangles). The onset latency, offset time, FWHM, and amplitude of each peak (purple) or trough (yellow) were calculated as described in the text. In this example, the onset and offset times of the trough happened to coincide with those of the half minumum.*

failed to cross our ±2 standard deviation criterion. We therefore conducted a separate analysis comparing the distribution of bins following the artifact window in each PSTH to a uniform distribution using a Kolmogorov-Smirnov goodness-of-fit test (KS test, $p<0.01$). This approach enabled identification of modulation too low in amplitude to be considered a peak or trough with our criteria. The results based on the 282 neuron-array pairs that met this non-uniform distribution criterion for significant modulation, presented as Supplemental Information, were generally consistent with the results obtained using peaks and troughs.

DATA AND SOFTWARE AVAILABILITY

Analysis-specific code and data are available by request to the Lead Contact.

Supplementary Information:

Direct Modulation assessed with KS test

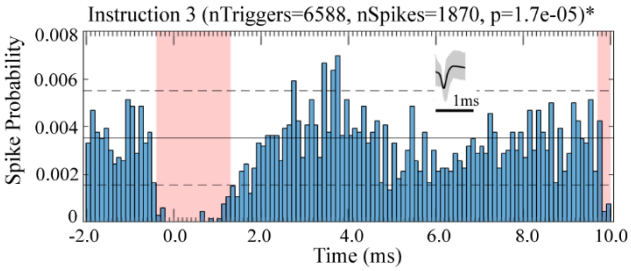

Figure S1: Example PSTH with modulation significant by KS test but without a significant peak or tough. *This PSTH constructed for a multi-unit from PM showed no peak or trough that met our criteria of > ±2 standard deviations for ≥ 3 consecutive bins, but did show modulation significant by the KS test (p=1.65e-05). Ch78U2, L, 20150729.*

For a number of neuron-array pairs the PSTH appeared to show modulation, but that modulation was not of sufficient amplitude to produce a peak or trough that exceeded ± 2 standard deviations of the baseline mean for three consecutive bins. An example is shown in Figure S1. We therefore performed a separate analysis using the Kolmogorov-Smirnov goodness-of-fit test (KS test) to evaluate the null hypothesis that the bins following the final artifact window did not differ from a uniform distribution. We chose a criterion of $p<0.01$, as we were testing >100 PSTHs in each monkey (see also Control for False Discovery Rate below). In the following supplemental analyses, PSTHs that were significantly non-uniform at this level (whether or not significant peaks or troughs were present) were considered to show direct modulation of the neuron by ICMS pulses delivered on the array.

We evaluated the percentage of neurons that were directly modulated by at least one instruction (i.e. by ICMS pulses delivered through electrodes on at least one S1 array). After Bonferroni correcting KS-test p-values for the multiple testing of 4 PSTHs in monkey L or 3 in monkey X, we counted neurons with at least one PSTH still significant at $p<0.01$. For M1 neurons, 37/38 (97%) in monkey L and 29/36 (81%) in monkey X were directly modulated by ICMS delivered through at least one S1 array. For PM neurons, 27/42 (64%) in monkey L and 30/33 (91%) in monkey X showed direct modulation. As might be expected, these percentages were slightly higher using the KS-test criterion as compared to the peak/trough criteria. Both methods showed that the majority of neurons recorded in both M1 and PM were directly modulated by ICMS delivered through at least one S1 array.

We also assessed convergence and divergence using the KS-test criterion to identify neuron-array pairs with direct modulation. These results, presented in both tabular (Figure S2) and graphic (Figure S3) form in parallel to Figures 4 and 5, confirm the convergence and divergence found using peaks and troughs. Effects of ICMS pulses delivered on multiple different arrays in S1 converged on many individual neurons in both M1 and PM. And conversely, effects from ICMS pulses delivered on any single S1 array diverged to neurons spread through wide territories in both M1 and PM.

M1
PM

Convergence

Monkey L

# Units	Array	# S1-Arrays Producing DM: 0	1	2	3	4
11	G	0%	55%	9%	0%	36%
5	I	0%	0%	40%	20%	40%
8	J	0%	0%	0%	25%	63%
15	K	7%	20%	13%	0%	60%
9	A	56%	33%	0%	11%	0%
7	B	29%	57%	0%	0%	14%
12	C	17%	25%	33%	8%	17%
13	D	31%	23%	15%	31%	0%

M1 vs. PM: p=6.1e-5, χ^2-test

Monkey X

# Units	Array	# S1-Arrays Producing DM: 0	1	2	3
5	F	0%	0%	20%	80%
11	G	0%	36%	18%	45%
2	H	0%	0%	0%	100%
18	I	33%	17%	33%	17%
12	C	0%	50%	42%	8%
18	D	17%	44%	17%	22%

M1 vs. PM: p=0.067, χ^2-test

Divergence

Monkey L

# Units	Array	S1-ICMS Arrays: M	N	O	P
11	G	100%	36%	45%	36%
5	I	40%	100%	80%	80%
8	J	75%	88%	75%	88%
15	K	80%	60%	87%	60%
9	A	44%	11%	11%	0%
7	B	43%	43%	14%	14%
12	C	67%	67%	25%	25%
13	D	54%	31%	38%	23%

M1 vs. PM: p=7.3e-10, χ^2-test

Monkey X

# Units	Array	S1-ICMS Arrays: K	L	O
5	F	100%	80%	100%
11	G	100%	64%	45%
2	H	100%	100%	100%
18	I	50%	67%	17%
12	C	100%	50%	8%
18	D	83%	39%	22%

M1 vs. PM: p=0.12 χ^2-test

Figure S2. Percentages of units directly modulated by ICMS pulses on each S1 array based on KS test. *For convergence tables (left), each entry contains the percent of units on each M1 (blue) and PM (green) array that were directly modulated (as assessed with the KS-test) by ICMS pulses delivered through different numbers of S1 arrays from 0 to 4. For divergence tables (right), each entry contains the percent of units recorded from each M1 or PM array that were directly modulated (by KS test) by ICMS pulses delivered through the indicated S1 array. All entries are color coded on a scale from white (0%) to dark blue/green (100%, M1/PM). Results for monkey L are displayed above and results for monkey X are displayed below.*

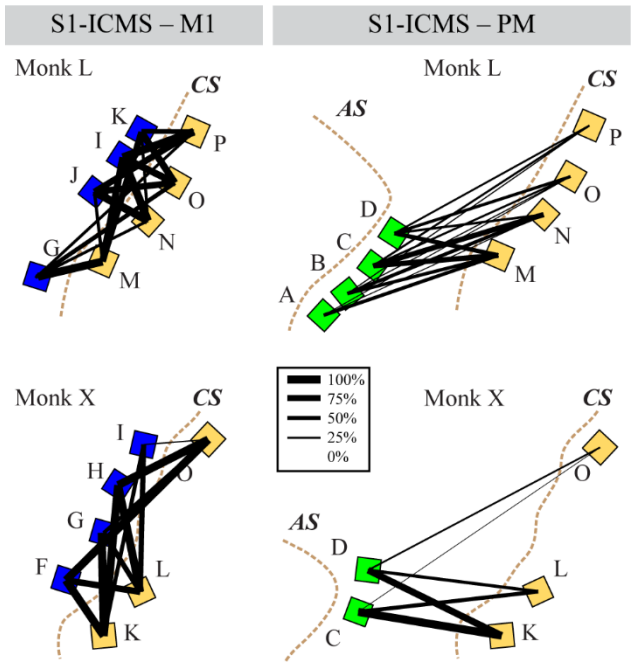

Figure S3. Graphic topography maps of direct modulation effects from each S1-ICMS array based on KS test. *Each square represents an FMA implanted in PM (green), M1 (blue) or S1 (yellow). The thickness of each solid black line is proportional to the percentage of units recorded from each M1 or PM array that were directly modulated by ICMS pulses delivered through the connected S1 array, as assessed with the KS-test. The letters next to the arrays correspond to those in Figure S2. Brown dotted lines indicate sulci: Arcuate Sulcus (AS) and Central Sulcus (CS).*

Control for False Discovery Rate

As a control, we constructed PSTHs using spike trains from visually-instructed trials in which no modulation could have been produced by ICMS pulses. These PSTHs were triggered on "blanking windows" that mimicked the pulse artifacts in ICMS-instructed trials. Like the recorded ICMS pulse artifacts, the blanking windows applied to visually-instructed trials started at the time of instruction onset, proceeded at the same inter-pulse interval as ICMS pulses, and ended at the time the monkey completed the movement, beginning the final hold. The width of the blanking windows matched the width of the final artifact window calculated from ICMS-instructed trials of the same neuron-array pair. Any spikes occurring during the blanking windows were removed from analysis of the visually-instructed spike trains, mimicking collisions between spikes and ICMS artifacts (Fig. S4A). This blanking procedure led to the removal of 16.6% of spikes occurring during visual instructions for monkey L, and 13.5% for monkey X. Figure S4B shows an example visual-instruction control PSTH for the same neuron illustrated in Figure 7. The control PSTH using data recorded during trials of visual instruction 1 had no significant modulation as assessed with either the peak/trough criteria or the KS test (p = 0.44).

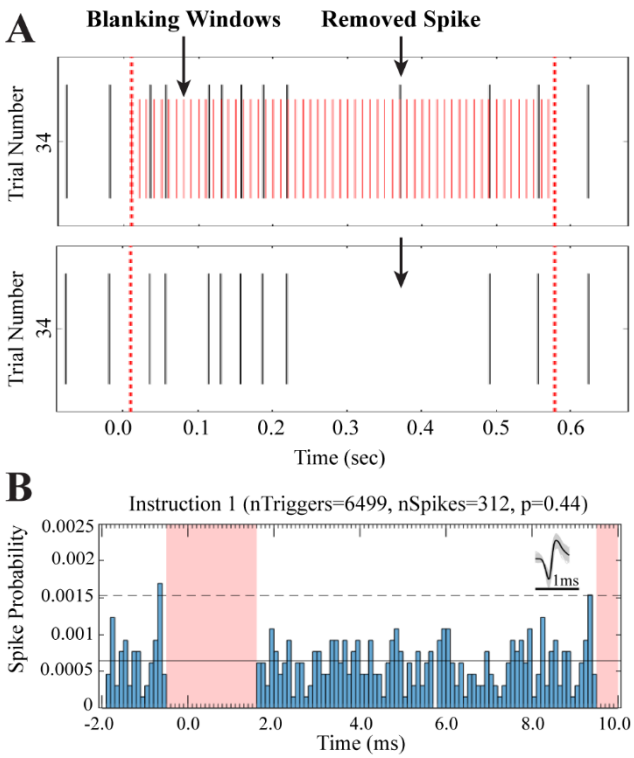

Figure S4: Building negative control PSTHs with blanking windows applied to spike trains from visually instructed trials. ***A)*** *A single-trial raster of spikes (vertical black lines) from a visually-instructed trial, aligned at the instruction onset (0sec). Red dashed lines indicate the times of instruction onset (left) and offset (right) Shorter red solid lines represent blanking windows occurring at the same frequency as stimulus artifacts recorded on this channel during ICMS trials. Only one spike collided with a blanking window and therefore was removed from the spike train.* ***B)*** *Negative control PSTH of same neuron-array pair as displayed in Figure 7, but using only data from visually instructed trials and triggered on blanking windows shown in A. No significant peak or trough is present, nor was the KS test significant (p=0.62). Note that reaction times were typically shorter on visually-instructed trials than ICMS-instructed trials leading to less nTriggers, but still a sufficient amount to capture direct modulation if it were present.*

We constructed such a visual-instruction control PSTH for each of the 152 M1 neuron-array pairs and 168 PM pairs from monkey L, and for each of the 108 M1 and 99 PM neuron-array pairs from monkey X analyzed in the main Results. Across all these visual-instruction control PSTHs, only 1.1% in monkey L and 1.2% in monkey X tested positive for direct modulation using the KS test criterion ($p<0.01$). Similarly, a peak or trough exceeding ±2 standard deviations of the baseline mean was found in only 4.7% of the visual-instruction control PSTHs from monkey L and 7.2% from monkey X. Both our KS-test criteria and our peak/trough criteria thus provided an acceptable false discovery rate.